Journal of Radioanalytical and Nuclear Chemistry (2019) 320:733–739
https://doi.org/10.1007/s10967-019-06545-2

Synthesis and phase structure of $(Cs_{0.8-x}Ba_{0.4+x})(Al^{3+}_{1.6+x}Ti^{4+}_{6.4-x})O_{16}$ ceramics using sol-spray pyrolysis route for immobilizing radioactive cesium

Yushan Yang[1] · Xiaodong Xie[1] · Xiaoyong Yang[1] · Xirui Lu[1] · Ke Yu[1] · Lingshuang Li[1] · Xueli Wang[1] · Xiaofen Wang[1] · Jiang Ma[1] · Linyan Li[2]

Received: 27 January 2019 / Published online: 6 May 2019

Abstract
In this paper, a sol-spray pyrolysis route was employed to fabricate (Cs, Ba)-hollandite ceramic waste forms. The high-phase purity $(Cs_{0.8-x}Ba_{0.4+x})(Al_{1.6+x}Ti_{6.4-x})O_{16}$ $(0 \le x \le 0.4)$ ceramics were synthesized at 1050 °C using the produced powders by sol-spray pyrolysis. The results show that all samples show tetragonal hollandite with rod morphology. Additionally, the sintered (Cs, Ba)-hollandite ceramics exhibit a good chemical durability. The normalized release rates of Cs and Ba were $< 10^{-2}$ g m^{-2} d^{-1} after 14 days. These results indicate that hollandite ceramics are promising candidate for immobilizing radioactive cesium.

Keywords Hollandite · Cesium immobilization · Spray pyrolysis · Microstructure

Introduction

Hollandites with general formula $A_2B_8O_{16}$ have long been consider as possible hosts for immobilization of radioactive cesium because of their high chemical durability, good thermal stability and high radiation resistance [1–3]. Due to excellent structural tolerance, hollandite-type oxides can accommodate larger A^+ or A^{2+} cations (Rb^+, Cs^+ and Ba^{2+}) at A-site, while the B-site is occupied by tri- and tetra-valent cations such as Al^{3+}, $Fe^{3+,}$ Ti^{3+} and Ti^{4+} etc. [4, 5]. Moreover, the charge compensation in hollandite lattice could be achieved through reduction of Ti^{4+} to Ti^{3+} [6], suggesting that the hollandite ceramics are a promising host for immobilizing radioactive Cs.

Various techniques have been employed to fabricate high quality hollandite ceramics, such as hot-pressure sintering, melting process and sol–gel method, etc. Unfortunately, some key problems should be solved in these methods. For instance, a higher pressure of about 40 Mpa is required in hot pressing sintering [7]. On the other hand, a higher temperature of above 1500 °C is requested in the melting process [8]. Last but not least, the pH and ageing time need to be controlled by using the sol–gel method [9]. Comparing with the shortages in these methods, spray pyrolysis (SP) has its own priorities in continuous, simple and inexpensive characteristics [10, 11]. Powders with uniformly homogeneity and good dispersity were prepared by atomizing a precursor solution with SP technology [12–14]. It indicates that the high quality hollandite ceramics are expected to be synthesized using the generated powders by SP at a lower sintering temperature for immobilizing volatile radioactive cesium.

In our present work, the high purity $(Cs_{0.8-x}Ba_{0.4+x})(Al_{1.6+x}Ti_{6.4-x})O_{16}$ ceramics were synthesized firstly from powder prepared by a spray pyrolysis process. Then substitution effects of Ba^{2+} for Cs^+ on the crystalline phase, morphology and chemical durability of the as-prepared (Cs, Ba)-hollandite samples were investigated in details. Finally, a summary of the study is given.

✉ Yushan Yang
yys168994@126.com

[1] School of National Defense Science and Technology, Southwest University of Science and Technology, Mianyang 621010, People's Republic of China

[2] Institute of Nuclear and New Energy Technology, Tsinghua University, Beijing 100084, People's Republic of China

Experimental procedures

Materials preparation

A homemade spray pyrolysis system was employed to prepare primary hollandite powders. The self-assembly SP equipment mainly included an atomization device, an air extractor, a resistance heating furnace, and a powder collector. In a typical process, the overall solution concentration was fixed at 0.1 mol L^{-1}. The solution comprised of Cs^+, Al^{3+} and Ba^{2+} was prepared by dissolving $CsNO_3$, $Al(NO_3)_3{\cdot}9H_2O$ and $Ba(NO_3)_2$ in distilled water, respectively. 100 mL of ethanol and 10 mL nitric acid are mixed in a 200 mL flask. 6.8 mL tetrabutyl titanate ($Ti(OC_4H_9)_4$) is dissolved in the nitric acid alcohol solution to restrain hydrolyzation of the tetra-n-butyl titanate, and dilute with ethanol to 200 mL with stirring for 30 min. After that, the precursor solution with nominal compositions of $(Cs_{0.8-x}Ba_{0.4+x})(Al_{1.6+x}Ti_{6.4-x})O_{16}$ was obtained by mixing the two solutions prepared before. Then citric acid and polyethylene glycol were added to the mixed solution in proportions of 8 and 5 g per 100 mL solution and was stirred for 2 h. Precursor powders were produced in the self-assembly SP equipment at 400 °C in air atmosphere. To remove residual organic species, the as-prepared powder was heated at 800 °C for 2 h. Finally, the post-treated powders were pressed into pellets 12 mm in diameter and 3 mm in thickness at the pressure of 12 MPa using a hydraulic press and sintered in air at 1050 °C for 5 h.

Sample characterization

The phase structure of the sintered (Cs, Ba)-hollandite ceramics was identified by X-ray diffraction (XRD) using Cu K_α radiation. The Raman spectra of specimens in the range of 100–800 cm^{-1} was recorded with the laser Raman spectrometer (InVia, UK) using 532 nm light from an argon laser. The morphology of the samples sintered was observed using field scanning electron microscopy (FSEM, ZEISS ULTRA 55). A transmission electron microscopy (TEM) sample was prepared by crushing ceramic fragments in ethanol and depositing a drop of suspension on a holey-carbon film. The microstructural information of the sample was observed by transmission electron microscopy (TEM, Libra 200 FE, Germany). Energy-dispersive X-ray spectroscopy (EDX), attached to the TEM equipment, was used to identify the chemical composition of the observed sample. A leaching test was conducted to examine Cs and Ba leaching from the synthesized samples using a modified MCC-1 method. The synthesized (Cs, Ba)-hollandite ceramic waste forms were suspended in a deionized water in a closed Teflon vessel. Then the vessels are placed into an oven maintained at a constant temperature of 90 ± 2 °C for a period of 1–21 days. After leaching, the concentrations in the leachant are detected by an inductively coupled plasma mass spectrometry (ICP-Mass, Agilent 7700x, Agilent, U.S.). The normalized elemental leach rate (NL_i, g m^{-2} d^{-1}) was calculated according to the following Eq. (1):

$$NL_i = \frac{C_i \cdot V}{SA \cdot f_i \cdot t_n} \tag{1}$$

where C_i (g m^{-3}) is the concentration of element i in the leachate, V (m^3) is the volume of the leachates, SA (m^2) is the surface area of the leach sample, f_i (wt%) is the mass fraction of element i in the ceramics and t_n (d) is the leaching time.

Results and discussion

Phase and structural stability

Figure 1 shows the XRD patterns of $(Cs_{0.8-x}Ba_{0.4+x})(Al_{1.6+x}Ti_{6.4-x})O_{16}$ ceramics with various compositions. It can been found that all samples are of well-developed crystalline structure, with distinct diffraction peaks corresponding to the intense reflections of hollandite, suggesting the high-phase purity (Cs, Ba)-hollandite solid solution has been formed at 1050 °C for 5 h and that the Cs^+ and Ba^{2+} ions are successfully incorporated into hollandite lattice. Furthermore, the observed equivalent Bragg reflections are shifted continuously towards higher angles with decreased cesium content (right part of Fig. 1). It can be explained that a decrease in unit cell volume resulted from the decreased ionic size of Ba^{2+} (1.42 Å) at the A site compared with that of Cs^+ (1.74 Å), in accordance with the previous results [2, 6].

It is worth noting that elemental Cs and most cesium compounds are volatile in the higher temperature (> 900 °C) [15, 16]. The synthesis of Cs-host at lower temperature (1050 °C) is conducive to preventing Cs volatilization during fabrication and further confirmed by EDX results (Fig. 5f). To the best of our knowledge, the (Cs, Ba)-hollandite ceramics were prepared at 1200–1250 °C by an alkoxide nitrate precursor route [17, 18], a hot presses sintering [19, 20] or a solid state reaction [18, 21]. Furthermore, a water-soluble $CsAlTiO_4$ phase is usually present in this system [15], which would affect the long-term chemical stability of the radioactive cesium waste forms [22]. Compared to coarser powders used in the solid state method, a submicron or nanometer size powders with excellent compositional homogeneity were generated from a precursor solution by sol-spray pyrolysis [12, 14, 23], which greatly eliminates component

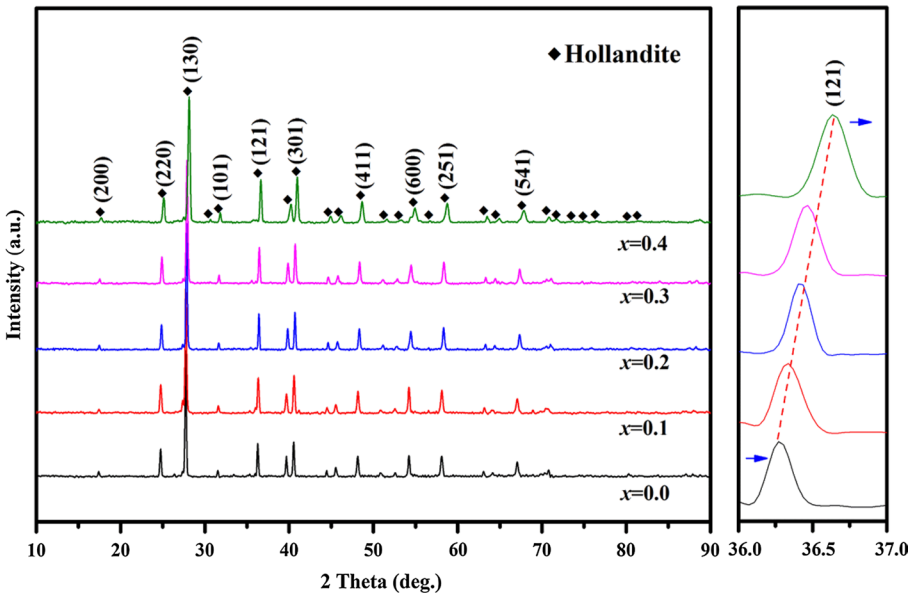

Fig. 1 XRD patterns of the $(Cs_{0.8-x}Ba_{0.4+x})(Al_{1.6+x}Ti_{6.4-x})O_{16}$ $(0 \le x \le 0.4)$ ceramics prepared by the Sol-SP method

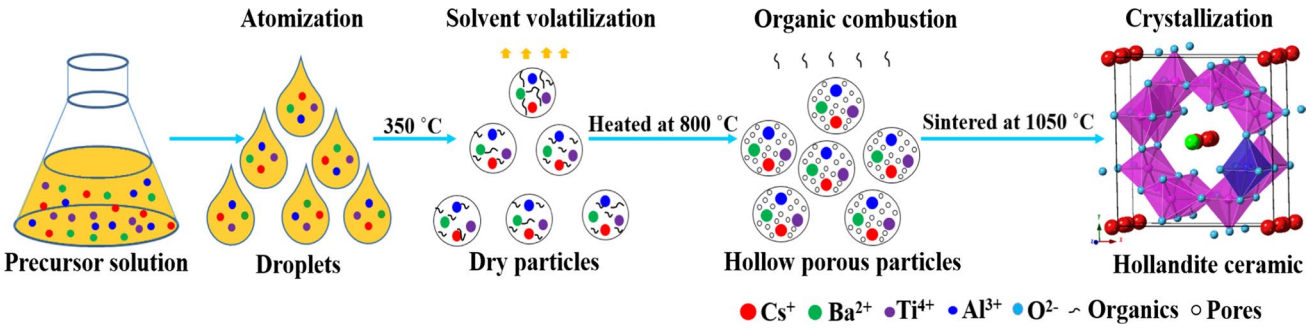

Fig. 2 Schematic illustration of the synthesis procedures of hollandite ceramic with SP

inhomogeneity appeared in solid state method. As shown in Fig. 2, the highly sinterable powders are obtained from the atomized droplets, improving the difference in setting time for precipitation of different components [24]. Moreover, previous results indicated that the high-quality powders promote the diffusion of particles at short range in the sintering process [25]. Therefore, the high purity hollandite ceramics are synthesized by Sol-SP only after the as-prepared powders sintered at 1050 °C for 5 h.

In the hollandite $A_2B_8O_{16}$, the structure can adapt to a tetragonal or monoclinic symmetry, depending on the mean radius ratio of cations in the A and B sites. For $(Cs_{0.8-x}Ba_{0.4+x})(Al_{1.6+x}Ti_{6.4-x})O_{16}$ solid solution, the ionic radius of Al^{3+} and Ti^{4+} are 0.585 and 0.605 Å, while that of Cs^+ and Ba^{2+} are 1.74 and 1.42 Å [26], respectively. The chemical difference between Cs and Ba are likely to impair the stability of the hollandite matrix. The structural stability of $A_2B_8O_{16}$ hollandite can be predicted using the radius ratio tolerance factor t_H following Eq. (2) defined by Kesson and White [27]:

$$t_H = \frac{\left[\left(r_A + r_O\right)^2 - \frac{1}{2}\left(r_B + r_O\right)^2\right]^{1/2}}{\sqrt{\frac{3}{2}}\left(r_B + r_O\right)} \quad (2)$$

where r_A is the average A-site cation radii, r_B is the average B-site cation radii, and r_O is the oxygen ion radius (1.4 Å). The average ionic radius of r_A and r_B in $(Cs_{0.8-x}Ba_{0.4+x})(Al_{1.6+x}Ti_{6.4-x})O_{16}$ $(0 \le x \le 0.4)$ compositions are estimated using the following Eqs. (3) and (4):

$$r_A = (0.8 - x)r_{Cs} + (0.4 + x)r_{Ba} \quad (3)$$

$$r_B = (1.6 + x)r_{Al} + (6.4 - x)r_{Ti} \quad (4)$$

The calculated results of t_H and r_B/r_A were collected in Table 1 and the calculated t_H as a function of Cs content is depicted in Fig. 3.

Although the t_H values ranging from 0.93 to 1.16 were predicted to be a stable hollandite phase [27], Cs cannot substitute all Ba atoms in hollandite lattice because of size

Table 1 The tolerance factor of $(Cs_{0.8-x}Ba_{0.4+x})(Al_{1.6+x}Ti_{6.4-x})O_{16}$ $(0.0 \le x \le 0.4)$

Compositions	Mean r_A (Å)	Mean r_B (Å)	r_B/r_A	Tolerance factor (t_H)
$Cs_{0.8}Ba_{0.4}Al^{3+}_{1.6}Ti^{4+}_{6.4}O_{16}$	1.568	0.601	0.383	1.065
$Cs_{0.7}Ba_{0.5}Al^{3+}_{1.7}Ti^{4+}_{6.3}O_{16}$	1.542	0.601	0.389	1.053
$Cs_{0.6}Ba_{0.6}Al^{3+}_{1.8}Ti^{4+}_{6.2}O_{16}$	1.517	0.601	0.396	1.041
$Cs_{0.5}Ba_{0.7}Al^{3+}_{1.9}Ti^{4+}_{6.1}O_{16}$	1.491	0.600	0.403	1.029
$Cs_{0.4}Ba_{0.8}Al^{3+}_{2.0}Ti^{4+}_{6.0}O_{16}$	1.466	0.600	0.409	1.017

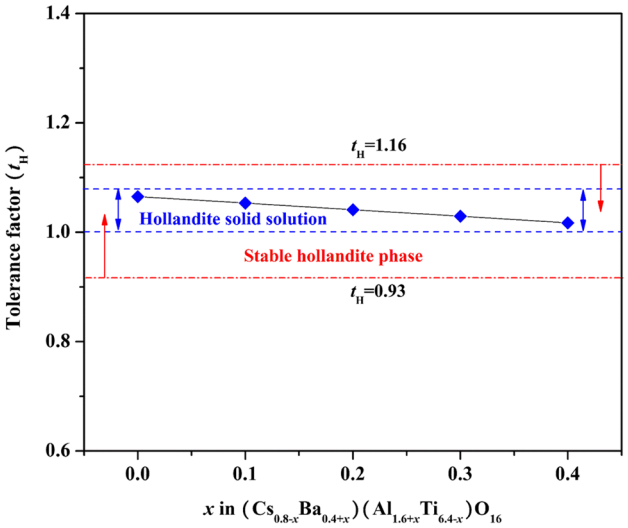

Fig. 3 The calculated t_H for $(Cs_{0.8-x}Ba_{0.4+x})(Al_{1.6+x}Ti_{6.4-x})O_{16}$ ceramics as a function of Cs content

constraints (r^{+}_{Cs}~1.74 Å > r^{2+}_{Ba}~1.42 Å) [4, 28]. As reported, the $\left[Cs_xBa_y\right]\left[\left(Al^{3+},Ti^{3+}\right)_{2y+x}Ti^{4+}_{8-2y-x}\right]O_{16}$ solid solution was only prepared in the range of $0.4 \le x, y \le 0.83$ [19], suggesting a finite (Cs, Ba)-hollandite solid solution is formed when the t_H value is very closer to 1 (Fig. 3). As seen in Table 1, the t_H values is limited to the range of $1.017 \le t_H \le 1.065$ in the $(Cs_{0.8-x}Ba_{0.4+x})(Al_{1.6+x}Ti_{6.4-x})O_{16}$ $(0 \le x \le 0.4)$ ceramics, and the variation of t_H is slighter than that of 0.93–1.16. Additionally, the value of r_B/r_A is less than 0.48 over the whole Cs content range. Thus, all compositions display a stable tetragonal structure, and supported by the XRD results.

Microstructure

To explore the substitution of Ba^{2+} for Cs^{+} on the structure and symmetry of the synthetic samples, the Raman spectra of $(Cs_{0.8-x}Ba_{0.4+x})(Al_{1.6+x}Ti_{6.4-x})O_{16}$ $(0.0 \le x \le 0.4)$ samples in the 100–800 cm^{-1} spectral region are shown in

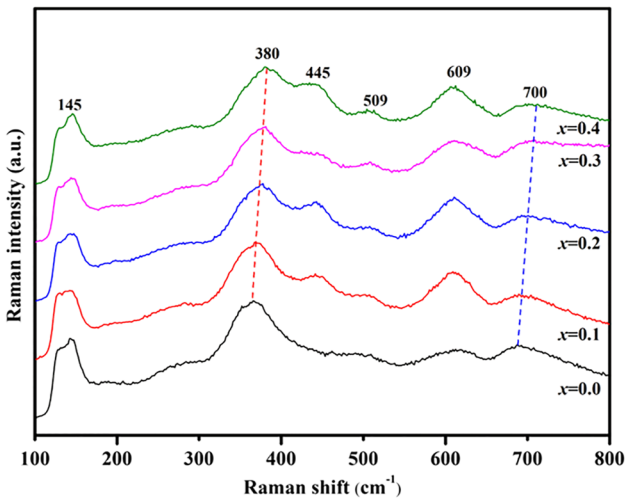

Fig. 4 Raman spectra of the $(Cs_{0.8-x}Ba_{0.4+x})(Al_{1.6+x}Ti_{6.4-x})O_{16}$ $(0 \le x \le 0.4)$ samples

Fig. 4. As seen in Fig. 4, six active modes are observed, at 145, 380, 445, 509, 609, 700 cm^{-1}. The observed bands are all indexed as Raman scattering from a tetragonal hollandite, in agreement with previous results reported [29, 30]. This result indicates that the synthetic (Cs, Ba)-hollandite system does not undergo the structural transition with the resultant substitutions of Ba^{2+} for Cs^{+} and Al^{3+} for Ti^{4+}. The band at 380 and 700 cm^{-1} are assigned to the A_g mode, corresponding to the symmetric stretching vibration of the (Al, Ti)–O bond [31, 32], whereas the band at 445 cm^{-1} is assigned to the E_g mode [33, 34]. Also noticed that the bands around 380 cm^{-1} and 700 cm^{-1} appear a slightly shift toward higher frequencies in the (Cs, Ba)-hollandite samples, which can be explained as the change of the strength of the O–B–O bond [32], due to the substitution of Al^{3+} for Ti^{4+}. Combined with the XRD results, it further confirms that the $\left(Cs_{0.8-x}Ba_{0.4+x}\right)\left(Al^{3+}_{1.6+x}Ti^{4+}_{6.4-x}\right)O_{16}$ solid solution retains a stable crystalline structure for the resultant substitutions of Ba^{2+} for Cs^{+} and Al^{3+} for Ti^{4+}.

Figure 5 displays the SEM, TEM and EDX images of the $(Cs_{0.6}Ba_{0.6})(Al_{1.8}Ti_{6.2})O_{16}$ sample. It can be found that the sintered sample exhibits the rod morphology (rod-like grains) through Fig. 5a, which is a typical hollandite structure [35–37]. The rod grains are further observed by TEM and the results are shown in Fig. 5b–d. It can been found that a well-developed rod grains with a length of ~ 300 nm is observed clearly (Fig. 5b). Furthermore, the clear orderly lattices with 0.711 nm illustrates the characteristic of tetragonal structure (Fig. 5c), assigned to the (110) lattice plane of hollandite phase [PDF#78-0018]. In the SAED pattern, the homogeneous periodic spots further confirm a tetragonal hollandite phase by the existence diffraction planes at (000), (130), (240) and (110) along the

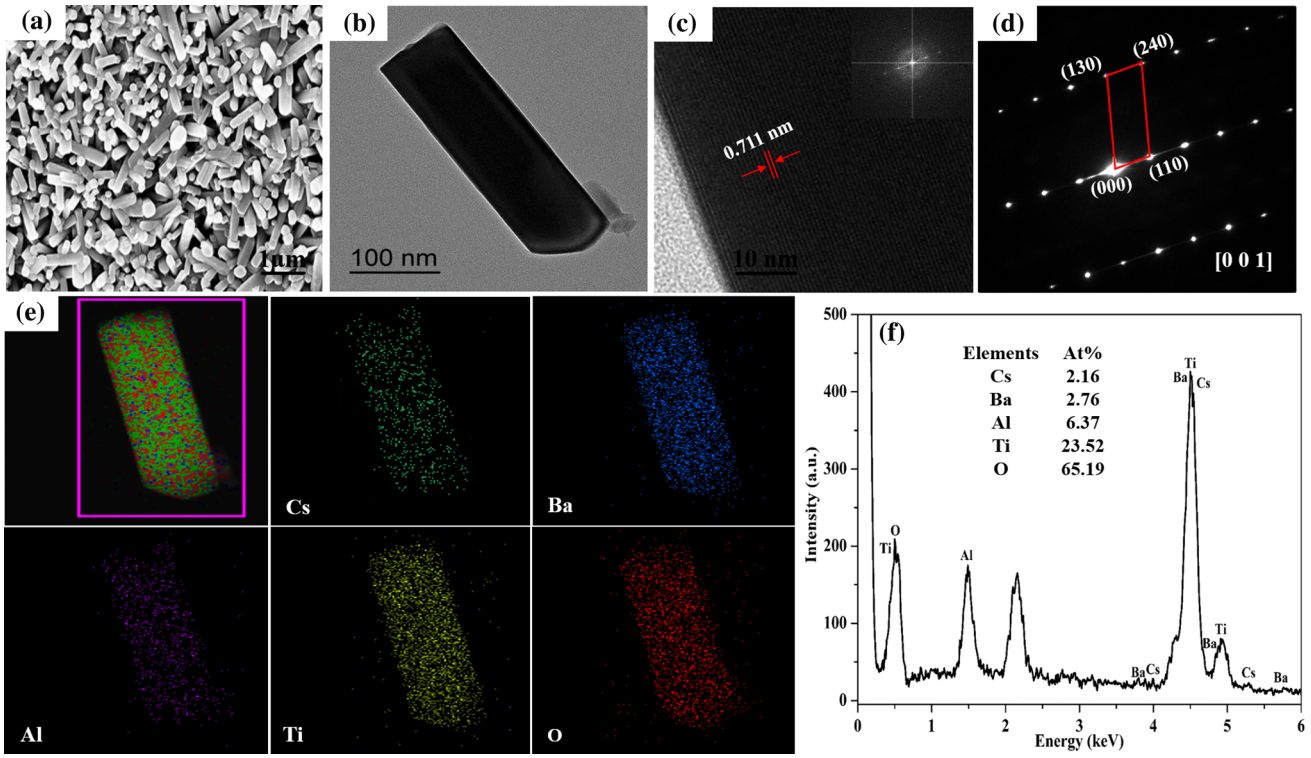

Fig. 5 SEM, TEM and EDX images of the $Cs_{0.6}Ba_{0.6}Al_{1.8}Ti_{6.2}O_{16}$ sample after sintering at 1050 °C for 5 h: **a** representative SEM image; **b** TEM image; **c** HRTEM image and the inset is FFT image; **d** SAED pattern, corresponding to **b**; **e** EDX elemental mappings and **f** EDX spectrum corresponding to **e**

[0 0 1] direction, in agreement with the results of XRD and Raman.

The EDX mapping images of $Cs_{0.6}Ba_{0.6}Al_{1.8}Ti_{6.2}O_{16}$ sample are also shown in Fig. 5. It can be found that the elements Cs, Ba, Al, Ti, and O are distributed uniformly throughout the entire crystal surface (Fig. 5e), and no evidence of the enrichment or deficiency of elements is observed in this mapping image. Moreover, EDX analysis indicates that the stoichiometry of Cs, Ba, Al, Ti, and O in the hollandite phase was 0.53, 0.68, 1.56, 5.77 and16 (Fig. 5f), which is close to the target values 0.6, 0.6, 1.8, 6.2 and16 (i.e., $Cs_{0.6}Ba_{0.6}Al_{1.8}Ti_{6.2}O_{16}$). However, the sum of the calculated positive charges is lower than 32. The positive charges deficient compared to oxygen rich could be explained by the following two reasons. First, the sum of positive charges decreases as metallic impurity (such as Co, Ni, Cu and Fe) deducted due to a chemical reagents impurity. Second, an oxygen rich or deficient presents usually in the oxides depending on the composition and process variables, and the low atomic number oxygen is very difficult to measure accurately. Thus, the positive charges of observed sample shows a slightly low than that of the expected composition.

It is worth noting that more than 85% of the targeted Cs concentration was retained in the observed hollandite sample, implying the sintering temperature (1050 °C) only leads to a slight loss of volatile Cs. However, only about 50% and 30% of the targeted Cs content remained by the solid state method and melt processing in previous reports [15, 20], due to a high fraction of cesium vaporized during higher temperature sintering (i.e., 1200 °C and 1675 °C, respectively). In Sol–SP, a lower sintering temperature employed, which effectually retards Cs volatilization during synthesis. Consequently, a good Cs retention is observed in the sintered ceramic samples, reflecting the key advantage of this method.

Durability

In order to evaluate the chemical durability of hollandite ceramic waste forms, a leaching test of the synthetic (Cs, Ba)-hollandite ceramics was carried out. The normalized elemental release rates of Cs and Ba in the $(Cs_{0.8-x}Ba_{0.4+x})(Al_{1.6+x}Ti_{6.4-x})O_{16}$ samples are shown in Fig. 6. It can be found that the normalized release rates of Cs and Ba decrease rapidly in the 1–7 days and decrease gradually after 7 days, and then nearly keep constant values after 14 days. The leach rates of Cs and Ba are about 7.8×10^{-3} g m^{-2} d^{-1} and 8.3×10^{-3} g m^{-2} d^{-1} in the 21st day, respectively, in agreement with previous results reported in hollandite

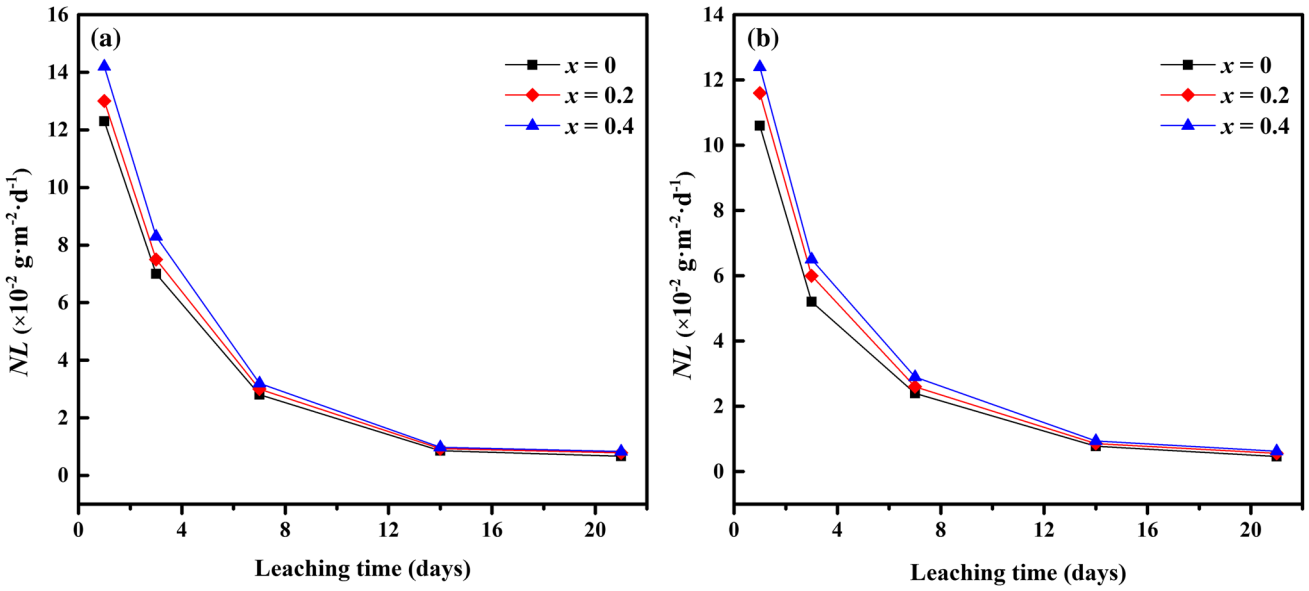

Fig. 6 Normalized release rates in $(Cs_{0.8-x}Ba_{0.4+x})(Al^{3+}_{1.6+x}Ti^{4+}_{6.4-x})O_{16}$ ceramics at 90 °C: **a** normalized release rates of Cs; **b** normalized release rates of Ba

ceramics [17, 38, 39]. Moreover, the normalized release rate of Ba is a slight lower than that of Cs for all time periods up to 21 days. The lower normalized release rate of Ba compared to Cs is ascribed to the larger bond energies of Ba–O than those of Cs–O in the hollandite structure [40].

It should be noted that the release rates of Cs is slight higher than the reported Cs release rates in hollandite ceramics [2], which can be attributed to a poor compactness of the products. As shown in Fig. 5a, the microstructural morphology is not compact in the bulk sample observed. The loose microstructure leads to a substantial increased reactive surface between ceramic sample and aqueous solution, and an increase of reactive surface sites in a ceramic host accelerates chemical attack during leaching test. As a result, a slightly high Cs leach is observed in the $(Cs_{0.8-x}Ba_{0.4+x})(Al_{1.6+x}Ti_{6.4-x})O_{16}$ ceramics. However, the Cs release rate is about two orders of magnitude lower than that of ~ 10 g m^{-2} d^{-1} in the glass waste forms [40–42], exhibiting a good chemical durability. Combined with XRD, Raman and TEM results, it can be concluded that hollandite ceramic waste forms can provide a stable treatment for immobilizing radioactive Cs.

Conclusions

In summary, a series of $(Cs_{0.8-x}Ba_{0.4+x})(Al_{1.6+x}Ti_{6.4-x})O_{16}$ $(0 \le x \le 0.4)$ ceramics were synthesized from powders fabricated by sol-spray pyrolysis. The effects of substitution of Ba^{2+} for Cs^{+} on phase structure and morphology of the (Cs, Ba)-hollandite ceramics were investigated using XRD, Raman, SEM and TEM–EDX. It was found that the resultant substitutions of Ba^{2+} for Cs^{+} and Al^{3+} for Ti^{4+} in the (Cs, Ba)-hollandite matrices do not cause substantial variation in phase structure and morphology. The synthetic (Cs, Ba)-hollandite ceramics show a tetragonal structure (*I*4/m) with a good Cs retention at 1050 °C for 5 h. Moreover, the normalized release rates of Cs and Ba in the (Cs, Ba)-hollandite waste forms were kept in a low value below 10^{-2} g m^{-2} d^{-1}, exhibiting a high Cs and Ba leach resistance.

Acknowledgements This work was supported by the National Natural Science Foundation of China (Nos. 41574100, 11705152, 21471088), the Doctor Research Foundation of Southwest University of Science and Technology (Nos. 15zx7129, 16zx715301), the Found by Longshan Academic Talent Research Supporting Program of Southwest University of Science and Technology (Nos. 18lzx511, 18lzx513) and the Postgraduate Innovation Fund of Southwest University of Science and Technology (No. 18ycx104).

References

1. Costa GCC, Xu H, Navrotsky A (2013) Thermochemistry of barium hollandites. J Am Ceram Soc 96:1554–1561
2. Carter ML, Vance ER, Mitchell DRG, Hanna JV (2002) Fabrication, characterization, and leach testing of hollandite, (Ba, Cs)$(Al, Ti)_2Ti_6O_{16}$. J Mater Res 17:2578–2589
3. Abdelouas A, Utsunomiya S, Suzuki T, Grambow B (2008) Effects of ionizing radiation on the hollandite structure-type: $Ba_{0.85}Cs_{0.26}Al_{1.35}Fe_{0.77}Ti_{5.90}O_{16}$. Am Mineral 93:241–247
4. Cheary RW, Kwiatkowska J (1984) An X-ray structural analysis of cesium substitution in the barium hollandite phase of synroc. J Nucl Mater 125:236–243

5. Carter ML, Withers RL (2005) A universally applicable composite modulated structure approach to ordered $Ba_xM_yTi_{8-y}O_{16}$ hollandite-type solid solutions. J Solid State Chem 178:1903–1914
6. Tumurugoti P, Clark BM, Edwards DJ, Amoroso J, Sundaram SK (2017) Cesium incorporation in hollandite-rich multiphasic ceramic waste forms. J Solid State Chem 246:107–112
7. Carter ML, Gillen AL, Olufson K, Vance ER (2009) HIPed tailored hollandite waste forms for the immobilization of radioactive Cs and Sr. J Am Ceram Soc 92:1112–1117
8. Amoroso J, Marra J, Conradson SD, Tang M, Brinkman K (2014) Melt processed single phase hollandite waste forms for nuclear waste immobilization: $Ba_{1.0}Cs_{0.3}A_{2.3}Ti_{5.7}O_{16}$; A = Cr, Fe, Al. J Alloys Compd 584:590–599
9. Wang MH, Zhang B, Zhou F (2014) Preparation and characterization of $CaCu_3Ti_4O_{12}$ powders by non-hydrolytic sol-gel method. J Sol-Gel Sci Technol 70:62–66
10. Marrero-López D, Romero R, Martín F, Ramos-Barrado JR (2014) Effect of the deposition temperature on the electrochemical properties of $La_{0.6}Sr_{0.4}Co_{0.8}Fe_{0.2}O_{3-\delta}$ cathode prepared by conventional spray-pyrolysis. J Power Sources 255:308–317
11. Cho JS, Rhee SH (2013) Formation mechanism of nano-sized hydroxyapatite powders through spray pyrolysis of a calcium phosphate solution containing polyethylene glycol. J Eur Ceram Soc 33:233–241
12. Sharma SC, Gokhale NM, Dayal R, Lal R (2002) Synthesis, microstructure and mechanical properties of ceria stabilized tetragonal zirconia prepared by spray drying technique. Bull Mater Sci 25:15–20
13. Gaudon M, Djurado E, Menzler NH (2004) Morphology and sintering behaviour of yttria stabilised zirconia (8-YSZ) powders synthesised by spray pyrolysis. Ceram Int 30:2295–2303
14. Chen CY, Tseng TK, Tsai SC, Lin CK, Lin HM (2008) Effect of precursor characteristics on zirconia and ceria particle morphology in spray pyrolysis. Ceram Int 34:409–416
15. Chevaldonnet AV, Caurant D, Dannoux A, Gourier D, Charpentier T, Mazerolles L, Advocat T (2007) Preparation and characterization of (Ba, Cs)(M, Ti)$_8O_{16}$ (M = Al^{3+}, Fe^{3+}, Ga^{3+}, Cr^{3+}, Sc^{3+}, Mg^{2+}) hollandite ceramics developed for radioactive cesium immobilization. J Nucl Mater 366:137–160
16. Lee JW, Lee DY, Lee YS, Yoon JY, Jeon SC, Lee JH, Hong SM, Cho YZ (2018) Cesium release during high-temperature pre-treatment of fuel fragments with a burn-up of 61 GWd/TU. J Radioanal Nucl Chem 317:15–23
17. Pham DK, Myhra S, Turner PS (1994) The surface reactivity of hollandite in aqueous solution. J Mater Res 9:3174–3182
18. Leinekugel-le-Cocq AY, Deniard P, Jobic S, Cerny R, Bart F, Emerich H (2006) Synthesis and characterization of hollandite-type material intended for the specific containment of radioactive cesium. J Solid State Chem 179:3196–3208
19. Kesson SE, White TJ (1986) $\left[Ba_xCs_y\right]\left[(Ti,\ Al)^{3+}_{2x+y}\ Ti^{4+}_{8-2x-y}\right]O_{16}$ synroc-type hollandites I. Phase chemistry. Proc R Soc Lond 405:73–101
20. Dandeneau CS, Hong T, Brinkman KS, Vance ER, Amoroso JW (2018) Comparison of structure, morphology, and leach characteristics of multi-phase ceramics produced via melt processing and hot isostatic pressing. J Nucl Mater 502:113–122
21. Grote R, Zhao M, Shuller-Nickles L, Amoroso J, Gong W, Lilova K, Navrotsky A, Tang M, Brinkman KS (2019) Compositional control of tunnel features in hollandite-based ceramics: structure and stability of $(Ba, Cs)_{1.33}(Zn, Ti)_8O_{16}$. J Mater Sci 54:1112–1125
22. Ringwood AE, Kesson SE, Ware NG, Hibberson W, Major A (1979) Immobilization of high level nuclear reactor wastes in synroc. Nature 278:219–223
23. Djurado E, Meunier E (1998) Synthesis of doped and undoped nanopowders of tetragonal polycrystalline zirconia (TPZ) by spray-pyrolysis. J Solid State Chem 141:191–198
24. Okuyama K, Lenggoro IW (2003) Preparation of nanoparticles via spray route. Chem Eng Sci 58:537–547
25. Jiang K, Liu SB, Ma GH, Zhao LL (2014) Microstructure and mechanical properties of $La_2Zr_2O_7$-$(Zr_{0.92}Y_{0.08})O_{1.96}$ composite ceramics prepared by spark plasma sintering. Ceram Int 40:13979–13985
26. Shannon RD (1976) Revised effective ionic radii and systematic studies of interatomic distances in halides and chalcogenides. Acta Cryst A 32:751–767
27. Kesson SE, White TJ (1986) Radius ratio tolerance factors and the stability of hollandites. J Solid State Chem 63:122–125
28. Bayer G, Hoffman W (1966) Complex alkali titanium oxides $A_x(B_yTi_{8-y})O_{16}$ of the α-MnO_2 structure-type. Am Mineral 51:511–516
29. Ohsaka T, Fujiki Y (1982) Raman spectra in hollandite type compounds $K_{1.6}Mg_{0.8}Ti_{7.2}O_{16}$ and $K_{1.6}A_{1.6}Ti_{6.4}O_{16}$. Solid State Commun 44:1325–1327
30. Shibata Y, Suemoto T, Ishigame M (1986) Raman scattering studies of mobile ions in superionic conductor hollandites. Phys Status Solidi B 134:71–79
31. Porto SPS, Fleury PA, Damen TC (1967) Raman Spectra of TiO_2, MgF_2, ZnF_2, FeF_2, and MnF_2. Phys Rev 154:522–526
32. Ohsaka T, Izumi F, Fujiki Y (1978) Raman Spectrum of anatase, TiO_2. J Raman Spectrosc 7:321–324
33. Roy N, Park Y, Sohn Y, Leung KT, Pradhan D (2014) Green synthesis of anatase TiO_2 nanocrystals with diverse shapes and their exposed facets-dependent photoredox activity. ACS Appl Mater Interfaces 6:16498–16507
34. Tian F, Zhang Y, Zhang J, Pan C (2012) Raman spectroscopy: a new approach to measure the percentage of anatase TiO_2 exposed (001) facets. J Phys Chem C 116:7515–7519
35. Yang XJ, Tang WP, Feng Q, Ooi K (2003) Single crystal growth of birnessite-and hollandite-type manganese oxides by a flux method. Cryst Growth Des 3:409–415
36. Xu Y, Wen Y, Grote R, Amoroso J, Shuller-Nickles L, Brinkman K (2016) A-site compositional effects in Ga-doped hollandite materials of the form $Ba_xCs_yGa_{2x+y}Ti_{8-2x-y}O_{16}$: implications for Cs immobilization in crystalline ceramic waste forms. Sci Rep-UK 6:27412
37. Cocco AP, Degostin MB, Wrubel JA, Damian PJ, Hong T, Xu Y, Liu YJ, Pianetta P, Amoroso JW, Brinkman KS, Chiu WKS (2017) Three-dimensional mapping of crystalline ceramic waste form materials. J Am Ceram Soc 100:3722–3735
38. Angeli F, Mcglinn P, Frugier P (2008) Chemical durability of hollandite ceramic for conditioning cesium. J Nucl Mater 380:59–69
39. Carter ML, Vance ER, Lumpkin GR, Loi E (2001) Aqueous dissolution of Rb-bearing hollandite and synroc-C at 90 °C. Mat Res Soc Symp Proc 663:381
40. Amini MM, Ahanj M (2000) Leach of cesium and barium from sol-gel derived zincborosilicate and borosilicate glasses. J Sol-Gel Sci Technol 18:119–125
41. Mitamura H, Banba T, Murakami T (1986) Effects of crystalline phases on leaching of a devitrified simulated high-level waste glass. Nucl Chem Waste Manag 6:223–231
42. Juoi JM, Ojovan MI, Lee WE (2008) Microstructure and leaching durability of glass composite wasteforms for spent clinoptilolite immobilization. J Nucl Mater 372:358–366